Empirical electron cross-field mobility in a Hall effect thruster

L. Garrigues,[1,a)] J. Pérez-Luna,[1,2] J. Lo,[1,2] G. J. M. Hagelaar,[1,2] J. P. Boeuf,[1,2] and S. Mazouffre[3]

[1]*Université de Toulouse, UPS, INPT, LAPLACE (Laboratoire Plasma et Conversion d'Energie), 118 route de Narbonne, F-31062 Toulouse Cedex 9, France*

[2]*CNRS, LAPLACE, F-31062 Toulouse, France*

[3]*ICARE (Institut de Combustion, Aérothermique, Réactivité et Environnement) IC, Avenue de la Recherche Scientifique, 45071 Orléans, France*

(Received 10 June 2009; accepted 14 September 2009; published online 5 October 2009)

Electron transport across the magnetic field in Hall effect thrusters is still an open question. Models have so far assumed $1/B^2$ or $1/B$ scaling laws for the "anomalous" electron mobility, adjusted to reproduce the integrated performance parameters of the thruster. We show that models based on such mobility laws predict very different ion velocity distribution functions (IVDF) than measured by laser induced fluorescence (LIF). A fixed spatial mobility profile, obtained by analysis of improved LIF measurements, leads to much better model predictions of thruster performance and IVDF than $1/B^2$ or $1/B$ mobility laws for discharge voltages in the 500–700 V range. © *2009 American Institute of Physics*. [doi:10.1063/1.3242336]

Hall effect thrusters (HETs) are nowadays employed on board of geostationary satellites for station keeping and orbit control. In a HET, the thrust is provided by the acceleration of xenon ions generated by the efficient ionization of a xenon neutral flow in a $E \times B$ field discharge. A 5 kW class Hall thrusters is now developed in order to achieve orbital maneuvers for the next generation of large geosynchronous satellites.[1]

One-dimensional (axial[2,3]) and two-dimensional (axial-radial[4–7]) models have been developed to simulate the HET behavior for various operating conditions. Most of these numerical models use a hybrid approach, where ions and neutrals are simulated with particle methods, whereas electrons are treated as a collisional fluid. Because the xenon density drops by two orders of magnitude due to the strong ionization of the xenon flow, the classical collisional mobility cannot explain the electron transport across the magnetic field barrier in the exhaust region of the thruster channel. Anomalous transport has been put forward to explain the electron cross-magnetic field mobility. Fully kinetic particle-in-cell (PIC) simulations in the axial and azimuthal directions have demonstrated the existence of a turbulent azimuthal electric field that leads to a cross-magnetic field transport of the electrons.[8] Recently, a collective light scattering diagnostic has evidenced azimuthal fluctuations of the electron density in the same wavelength range as in PIC simulations.[9] However, a scaling law of the anomalous transport has not yet been proposed. Consequently, most of the hybrid models have adopted elementary formulas with tuned parameters to account for the anomalous electron transport.[5,6,10–12]

The electron mobility perpendicular to the magnetic field $\mu_{e,\perp}$ under the drift-diffusion approximation used in hybrid models is defined as

$$\mu_{e,\perp} = \frac{j_{e,\perp}}{en_eE_\perp + e\nabla_\perp(n_eT_e)}, \tag{1}$$

where e is the elementary electron charge and n_e, T_e, and $j_{e,\perp}$, are the electron density, temperature, and cross-field current density, respectively. $\nabla_\perp$ symbolizes the cross-field gradient and $E_\perp$ is the electric field perpendicular to the magnetic field. The direct determination of the electron mobility in Eq. (1) through the measurements of plasma properties is questionable. Intrusive probes may perturb the thruster operation, the data that are difficult to interpret in the region of strong magnetic field can also yield very noisy results.[13] The accuracy of the measurements is insufficient to extract a quantitative axial profile of the electron mobility.

The elementary theory links the electron mobility to the total electron momentum transfer frequency ν_m and to the cyclotron angular frequency Ω,

$$\mu_{e,\perp} = \frac{e}{m_e\nu_m}\frac{1}{1+(\Omega/\nu_m)^2}, \quad \Omega = \frac{eB}{m_e}, \tag{2}$$

where m_e is the electron mass and B is the magnetic field magnitude. Up to now, in hybrid models, the total electron momentum transfer frequency ν_m is an effective collision frequency including the electron-atom collisions (frequency ν_a), electron-ion collisions (frequency ν_c), electron-wall collisions (frequency ν_w), and Bohm-like transport (frequency ν_{Bohm}). The total electron momentum transfer frequency in Eq. (2) is written as the sum of each contribution; therefore, $\nu_m = \nu_a + \nu_c + \nu_w + \nu_{\mathrm{Bohm}}$.[5,6,10–12] Elementary laws (with coefficients tuned to reproduce thruster performance) are used to account for electron-wall collisions as well as Bohm-like transport, leading to a mobility varying as $1/B^2$ and $1/B$, respectively.

In this letter, we show that nonintrusive laser induced fluorescence (LIF) measurements of the ion velocity distribution function (IVDF) allow us to infer the space distribution of the electron mobility in the direction perpendicular to the magnetic field. The results show that models assuming simple elementary scaling laws for the electron mobility are not able to reproduce experimental observations.

a)Electronic mail: laurent.garrigues@laplace.univ-tlse.fr.

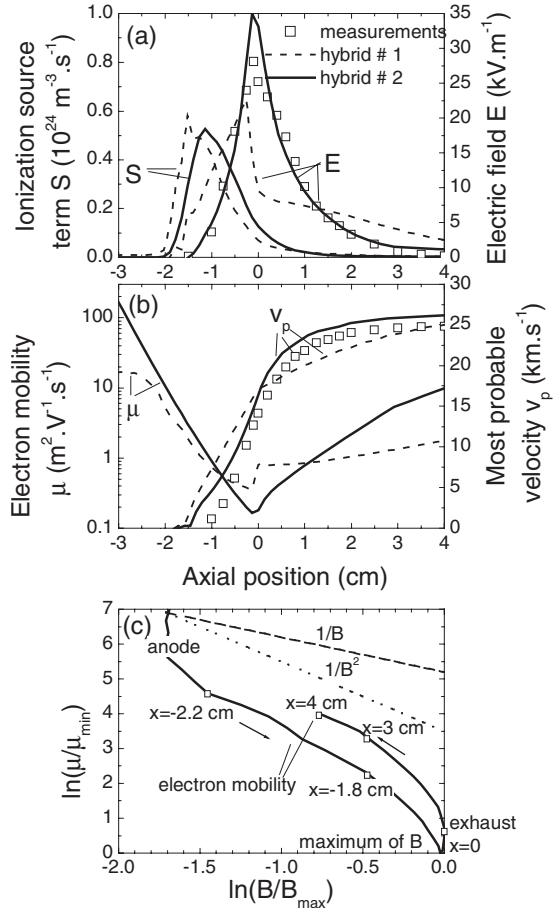

FIG. 1. Time-averaged profiles along the PPS®X000-ML thruster channel axis of (a) the electric field deduced from LIF measurements and the computed electric field profile and the calculated ionization source term and (b) the electron mobility perpendicular to the magnetic field and most probable ion velocity. (c) Electron mobility variations as a function of the magnetic field strength B; $1/B^n$ laws with $n=1$ and $n=2$ are also presented. Conditions are $U_d=500$ V and $m_a=6$ mg s^{-1}. The coil current is fixed at 17 A. The channel exit is at $x=0$.

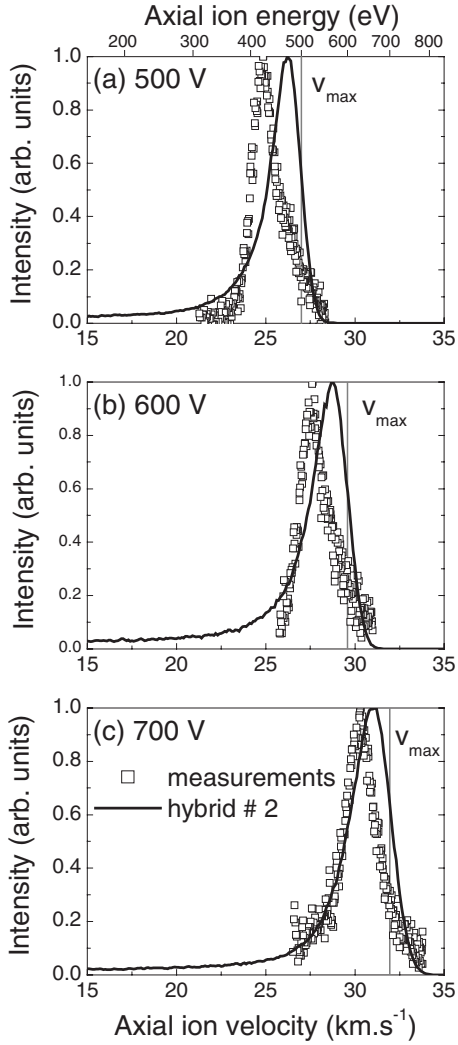

FIG. 2. IVDFs obtained by LIF measurements and calculated with the PPS®X000-ML at $x=4$ cm for (a) $U_d=500$ V, (b) $U_d=600$ V, and (c) $U_d=700$ V, and for $m_a=6$ mg s^{-1} (Ref. 19). The coil current is 17 A. The theoretical maximum axial velocity v_{max} is also shown.

Over the past 10 years, the time-averaged LIF technique has been extensively used and many measurements of the IVDF have been performed along the thruster channel centerline both inside and outside the thruster over a broad range of electrical power.[14–18] Recent improvements in the signal-to-noise ratio have been achieved.[19] In parallel, a technique based on the calculations of the moments of the Boltzmann equation has been recently proposed to extract the on-axis distribution of the electric field from well-defined LIF measurements.[20]

In Fig. 1(a), the experimental as well as the simulated time-averaged on-axis profiles of the axial electric field are shown together with the computed ionization source term. The results were obtained for the PPS®X000-ML thruster with a discharge voltage of 500 V and a xenon mass flow rate of 6 mg s^{-1}. In the calculations indicated as hybrid 1, we represent the anomalous electron transport mechanisms taking into account wall effects inside the channel with a collision frequency equal to $\nu_w=\alpha\nu_{\text{ref}}$ (with $\nu_{\text{ref}}=10^7$ s^{-1}) and outside the channel Bohm-like transport with an equivalent collision frequency $\nu_{\text{Bohm}}=K\Omega/16$. The adjustable coefficients are $\alpha=1.45$ and $K=0.2$, as in Ref. 10. The electron mobility profile calculated with Eq. (1) is plotted in Fig. 1(b). The use of empirical laws with $1/B^2$ (or $1/B$—not shown here) mobility inside the channel and $1/B$ outside the channel, as we have previously done with tunable coefficients, do not allow us to reproduce the measured profile of axial ion velocity. Koo and Boyd arrived at identical conclusions, in the context of the study of the University of Michigan/US Air Force P5 thruster.[5]

In the calculations labeled as hybrid 2, we have adjusted the anomalous electron mobility profile in order to match the experimental profile of the axial ion velocity [see Fig. 1(b)]. The shape of the calculated axial electric profile presented in Fig. 1(a) is now in agreement with the profile deduced from LIF measurements. Integrating the measured axial electric field profile leads to a potential drop much smaller than the discharge voltage (sheath falls). This explains the shift between the simulated and the measured most probable velocity (see Fig. 2). The fitted electron mobility profile (depending on the axial position) shown in Fig. 1(b) is in qualitative agreement with the measured profile in the P5 thruster.[5,21]

We have represent in Fig. 1(c) in log scale the variation in the adjusted electron mobility as a function of the magnetic field strength (normalized by the maximum of the magnetic field where the electron mobility is minimum). We also present in the same figure the $1/B^n$ laws for $n=1$ (Bohm

diffusion) and $n=2$ (classical and electron-wall diffusions). We can remark that inside the channel in the region of low magnetic field, the electron mobility profile follows a law very close to $n=2$; surprisingly, it is also the case outside the channel (beyond $x=3$ cm). In the region of high magnetic field, the variation in the adjusted electron mobility varies more quickly that $1/B^2$ or $1/B$.

The choice of tuned coefficients in the elementary laws ($1/B^2$ or $1/B$) used so far in hybrid models has influenced the dynamic behavior of the discharge, especially the magnitude of transit-time oscillations. The transit-time oscillations (100–500 kHz) are associated with the time needed by the ions to cross the acceleration layer. The visible consequence was noticed in the shape of IVDFs at the end of the acceleration layer where a large velocity dispersion was obtained.[11,12] In Fig. 2(a), we show the calculated and the measured IVDFs of the PPS®X000-ML thruster at $x=4$ cm (at the end of the acceleration layer, the reference axial position $x=0$ is at the exit plane) for discharge voltages in the range of 500–700 V, keeping the coil currents and the mass flow of neutrals constant. The empirical mobility profile is the same as in Fig. 1(b). The calculated IVDFs now match the measured IVDF (especially the broadening of the distribution). This suggests that the high-frequency dynamic behavior is correctly represented in the model. The theoretical maximum axial velocity an ion can reach for a given discharge voltage U_d is $v_{\max}=(2eU_d/m_{\mathrm{Xe}^+})^{1/2}$, where m_{Xe^+} is the ion mass. Both model and experiments confirm the existence of very fast ions with a velocity larger than $v_{\max}$ in the final part of the acceleration layer. This is clearly attributed to a "wave riding" phenomenon that makes possible for the ions to acquire a kinetic energy larger than the given potential energy $e\times U_d$.[11,12,17,19]

In this letter, we have demonstrated that laser spectroscopy is able to provide indirect information on the axial electron mobility profile. The results show that previous elementary laws ($1/B^2$ or $1/B$) with adjusted coefficients in order to match the correct "macroscopic" properties of the thruster (current, power, and performance) used so far in hybrid models fail to reproduce experimental observations such as the measured ion velocity profile. Fitting the calculated ion velocity profiles with the LIF measurements obtained at 500 V leads to a empirical steady spatial profile of the axial electron mobility that is able to reproduce the thruster properties and the measured ion velocity distribution functions, in the wide range of discharge voltages for the PPS®X000-ML thruster.

The adjusted electron mobility profile in this letter is in qualitative agreement with the calculated electron mobility from PIC simulations.[22] We now plan to use the PIC model in order to identify and understand the physical parameters that govern the anomalous electron transport. We also want to deduce from these calculations scaling laws of the electron mobility as a function of the discharge parameters in order to propose a less empirical description of the electron mobility in the hybrid model.

This work was performed in the frame of the joint-research program CNRS/CNES/Sncema/Universités No. 3161 "Propulsion par Plasma dans l'Espace" and by the TELIOPEH ("Transport ELectronique et IOnique dans les Propulseurs à Effet Hall") project funded by ANR (National Research Agency) under Contract No. ANR-06-BLAN-0171. J.P.-L. has benefited from a CNES/Snecma Ph.D. fellowship.

[1] S. Mazouffre, A. Lazurenko, P. Lasgorceix, M. Dudeck, S. d'Escrivan, and O. Duchemin, Proceedings of the Seventh International Symposium on Launcher Technologies, Barcelona, Spain, 2–5 April 2007 (unpublished), Paper No. 0-25.
[2] S. Barral, K. Makowski, Z. Peradynski, N. Gascon, and M. Dudeck, Phys. Plasmas **10**, 4137 (2003).
[3] J. P. Boeuf and L. Garrigues, J. Appl. Phys. **84**, 3547 (1998).
[4] G. J. M. Hagelaar, J. Bareilles, L. Garrigues, and J. P. Boeuf, J. Appl. Phys. **91**, 5592 (2002).
[5] J. W. Koo and I. D. Boyd, Phys. Plasmas **13**, 033501 (2006).
[6] M. K. Scharfe, N. Gascon, and M. A. Cappelli, Phys. Plasmas **13**, 083505 (2006).
[7] F. I. Parra, E. Ahedo, J. M. Fife, and M. Martinez-Sanchez, J. Appl. Phys. **100**, 023304 (2006).
[8] J. C. Adam, A. Heron, and G. Laval, Phys. Plasmas **11**, 295 (2004).
[9] S. Tsikita, N. Lemoine, V. Pisarev, and D. M. Gresillon, Phys. Plasmas **16**, 033506 (2009).
[10] C. Boniface, L. Garrigues, G. J. M. Hagelaar, J. P. Boeuf, D. Gawron, and S. Mazouffre, Appl. Phys. Lett. **89**, 161503 (2006).
[11] J. Bareilles, G. J. M. Hagelaar, L. Garrigues, C. Boniface, J. P. Boeuf, and N. Gascon, Phys. Plasmas **11**, 3035 (2004).
[12] G. J. M. Hagelaar, J. Bareilles, L. Garrigues, and J. P. Boeuf, J. Appl. Phys. **93**, 67 (2003).
[13] N. B. Meezan, W. A. Hargus, Jr., and M. A. Cappelli, Phys. Rev. E **63**, 026410 (2001).
[14] N. Dorval, J. Bonnet, J. P. Marque, E. Rosencher, S. Chable, F. Rogier, and P. Lasgorceix, J. Appl. Phys. **91**, 4811 (2002).
[15] W. A. Hargus, Jr. and C. S. Charles, J. Propul. Power **24**, 127 (2008).
[16] W. A. Hargus, Jr. and M. R. Nakles, IEEE Trans. Plasma Sci. **36**, 1989 (2008).
[17] D. Gawron, S. Mazouffre, N. Sadeghi, and A. Héron, Plasma Sources Sci. Technol. **17**, 025001 (2008).
[18] S. Mazouffre, D. Gawron, V. Kulaev, and N. Sadeghi, IEEE Trans. Plasma Sci. **36**, 1967 (2008).
[19] S. Mazouffre, V. Kulaev, and J. Pérez-Luna, Plasma Sources Sci. Technol. **18**, 034022 (2009).
[20] J. Pérez-Luna, G. J. M. Hagelaar, L. Garrigues, and J. P. Boeuf, Plasma Sources Sci. Technol. **18**, 034008 (2009).
[21] J. M. Haas and A. D. Gallimore, Phys. Plasmas **8**, 652 (2002).
[22] J. C. Adam, J. P. Boeuf, N. Dubuit, M. Dudeck, L. Garrigues, D. Gresillon, A. Heron, G. J. M. Hagelaar, V. Kulaev, N. Lemoine, S. Mazouffre, J. Pérez-Luna, V. Pisarev, and S. Tsikita, Plasma Phys. Controlled Fusion **50**, 124041 (2008).